Conditions for notch strength to be higher than static tensile strength in high–strength ductile cast iron

Tomohiro Ikeda[a,*], Nao–Aki Noda[b,*], Yoshikazu Sano[b]

[a] HINODE, Ltd., Azaiwasaki, Miyaki–cho, Miyaki–gun, Saga 849–0101, Japan
[b] Kyushu Institute of Technology, Sensui–cho, Tobata–ku, Kitakyushu, Fukuoka 804–8550 Japan

ARTICLE INFO

ABSTRACT

In this study, notch strength σ_B^{notch} was studied for a wide range of testing speed and temperature in comparison with the static tensile strength at room temperature $\sigma_{B,RT}^{smooth}$. High–speed tensile tests were conducted on high–Si ductile cast iron, conventional ferrite–pearlite ductile cast iron, and fully pearlitic ductile cast iron at a stroke speed ranging between 8.5×10^{-3} and 2.7×10^{2} mm/s (strain rate of 2.1×10^{-4} and 1.8×10^{1} s^{-1}) and temperature ranging between $-180\,°C$ and $22\,°C$. Then, σ_B^{notch} and $\sigma_{B,RT}^{smooth}$ were compared in terms of the strain rate-temperature parameter $R = T \ln (A/\dot{\varepsilon})$ to evaluate the combined influence of the strain rate $\dot{\varepsilon}$ and temperature T. It was found that the notch strength σ_B^{notch} can be expressed as a unique master curve in terms of R parameter for each material. Then, a notch–strengthening threshold criterion $R \geqq R_{th}$ was proposed to describe the lowest service temperature and highest strain rate that can be applied to the structural components. Under the condition $R \geqq R_{th}$, σ_B^{notch} is always larger than $\sigma_{B,RT}^{smooth}$, and therefore, notched components can be used safely. In other words, if $R \geqq R_{th}$, $\sigma_{B,RT}^{smooth}$ can be used to evaluate the notched components in machine design to prevent instantaneous fractures.

1. Introduction

Ductile cast iron is not an individual material but a part of a group of materials that can be produced with a wide range of properties by controlling their microstructure. Fig. 1 shows that the mechanical properties of even ferrite–pearlite ductile iron can be altered considerably to meet demanding requirements [1]. As shown in Fig. 1, a higher strength can be achieved by increasing the pearlite content in the ferrite–pearlite matrix. For example, the pearlite contents ranging between 45% and 55% correspond to a tensile strength of approximately 500 MPa, but the pearlite contents ranging between 80% and 90% correspond to a tensile strength of more than 700 MPa. The size and weight of various structures can be reduced using such high–strength materials.

In recent years, high–Si ductile cast iron, which is ferritic ductile iron strengthened by high–silicon solid solution, has attracted great attention, especially in Europe [2–5]. The section sensitivity of this material is low, which means that it provides nearly the same strength independent of product geometry. Furthermore, this material has a larger elongation and higher fatigue strength in comparison with the conventional ferrite–pearlite ductile cast iron of the same tensile strength [6]. These advantages indicate the potential of this new material for wide industrial application. However, one might think that this new material may have some disadvantages.

Fig. 2 compares the Charpy absorbed energy values of JIS–FCD500, JIS–FCD700 [6,7], and high–Si ductile cast iron, whose tensile

Nomenclature

|			
A	material constant value $= 10^8$ (s^{-1})	$u(t)$	stroke displacement (mm)
		$u(t)\,/\,t$	tensile speed (mm/s)
d	minimum test specimen diameter (mm)	T	temperature (K)
$K_t\dot{\varepsilon}$	strain rate concentration factor (–)	$\dot{\varepsilon}^{notch}$	strain rate in notched specimen (s^{-1})
ℓ	gauge length (mm)	$\dot{\varepsilon}^{smooth}$	strain rate in smooth specimen (s^{-1})
P	applied load (N)	ρ	notch root radius (mm)
P_{max}	maximum load obtained from the tensile test (N)	σ_B^{notch}	notch strength in notched specimen (MPa)
R	strain rate– temperature parameter (K)	σ_B^{smooth}	tensile strength in smooth specimen (MPa)
R_{th}	notch strengthening threshold (K)	$\sigma_{B,\,RT}^{smooth}$	static tensile strength at room temperature (MPa)
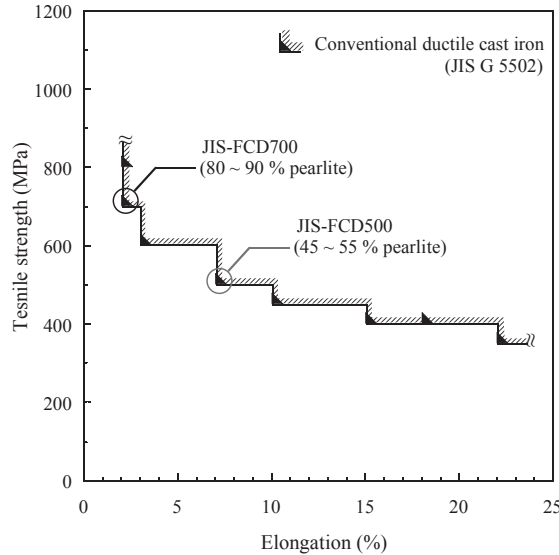
Fig. 1. Tensile strength and elongation of ferrite–pearlite ductile cast iron [1].
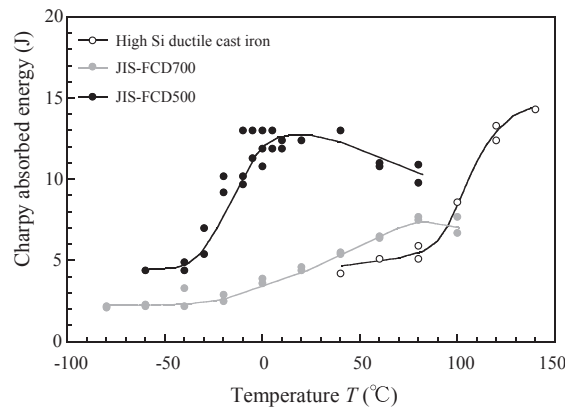

Fig. 2. Results of Charpy impact test of JIS–FCD500, JIS– FCD700 [6,7] and high–Si ductile cast iron, the tensile strength of which is nearly the same as that of JIS–FCD500.

strength is nearly the same as that of JIS–FCD500. As shown in Fig. 2, the Charpy absorbed energy is considerably low in the case of JIS–FCD700 [6,7] and high–Si ductile cast iron over the most parts of the temperature region. This is the main reason for the limited industrial application of high–strength grade ductile cast iron. It should be noted that the Charpy impact test is unsuitable from the viewpoint of selecting the structural materials because the impact speed is usually too high to evaluate real failures of real products. The toughness and strength of ductile cast iron depends strongly on the strain rate and temperature [8–11], and the ductile–brittle transition temperature increases with increasing the strain rate [9]. Moreover, the Charpy absorbed energy cannot be used directly in machine design in a manner that is different from the commonly used tensile strength and yield strength criteria. By considering these

disadvantages, high–speed tensile testing is now being recognized as a standard dynamic strength test to evaluate impact strength [12–16].

Therefore, in this paper, the notch strength and smooth tensile strength are compared in the case of instantaneous fracture, as shown in Fig. 3. If the notch strength is sufficiently high, tensile strength can be used as the notch strength in machine design. In this study, therefore, high–speed tensile tests are conducted at a stroke speed of 8.5×10^{-3}–2.7×10^{2} mm/s (strain rate of 2.1×10^{-4}–1.8×10^{1} s^{-1}) and temperature of -180 °C–22 °C. Then, notch strength and smooth tensile strength are discussed in terms of the strain rate–temperature parameter $R = T \ln (A/\dot{\varepsilon})$, $A = 10^{8}$ s^{-1} (const.), to evaluate the combined influence of strain rate $\dot{\varepsilon}$ and temperature T.

Note that Charpy impact test has been used for many years as a unique method in many industries to ensure the safety of structural materials including ductile cast irons under lower temperature. To propose an alternative method by extending Charpy under different impact speed, a similar notch shape of Charpy will be focused. However, impact bending like Charpy is not suitable for machine design because the bending strength cannot be used conveniently in contrast to the tensile strength and yield strength. Therefore, in this paper, a notched round bar specimen having a specific notch shape will be considered under various tensile speed test and various temperature. The obtained results will be compared each other under different conditions. The notch strength will be also compared with the tensile strength of smooth specimen.

2. Experimental procedures

2.1. Preparation of specimens

In this study, we considered ferrite–pearlite ductile cast irons JIS–FCD500 with tensile strength $\sigma_{B, RT}^{smooth} = 500$ MPa, JIS–FCD700 with tensile strength $\sigma_{B, RT}^{smooth} = 700$ MPa, and fully pearlitic ductile cast iron (PDI) with tensile strength $\sigma_{B, RT}^{smooth} = 900$ MPa. In addition, we consider high–Si ductile cast iron, which is now expected to be used as a material for structural components [3–5]. Cast specimens of those materials were prepared to investigate the notch strength. Fig. 4 shows the heat treatment procedure for obtaining PDI. All test specimens, such as JIS No.4 tensile test specimen and high–speed tensile test specimen, were taken from JIS Type II Y–shaped blocks JIS–G 5502 [1] of the highlighted sections in gray with dimensions $40 \times 25 \times 250$ mm, as shown in Fig. 5.

Table 1 presents the chemical compositions of specimens. Table 2 and Fig. 6 show and summarize, respectively, the results of microstructure analysis according to JIS–G5502. As presented in Table 2, all specimens have nearly the same graphite structures. The high–Si ductile cast iron has a fully ferritic matrix. JIS–FCD500 and JIS–FCD700 have pearlite ratios of 52.2 and 83.6, respectively. PDI has a fully pearlitic matrix. Table 3 shows the static tensile property of JIS No.4 steel obtained by the tensile test specimen with a diameter of 14 mm, gage length of 50 mm, and the procedure prescribed in JIS–Z 2241 standard.

2.2. High–speed tensile test

High–speed tensile tests were conducted on smooth specimens and notched round bar specimens, as shown in Fig. 7. The notch has the same shape and dimensions as those of the Charpy V–notch specimen. Note that this notch root radius $\rho = 0.25$ mm is considerably sharper than the real radius of casting products. Moreover, note that the notch depth of 2 mm is considerably deeper than the depth of surface scratches on the cast products. In this way, although the notch geometries are quite different from practical use, in this study, Fig. 7(b) is proposed as an alternative specimen used in high speed tensile test, which may replace Charpy impact testing. The tests were carried out using an electrohydraulic servo testing machine at stroke speed ranging between 8.5×10^{-3} and 2.7×10^{2} mm/s (strain rate of 2.1×10^{-4} and 1.8×10^{1} s^{-1}) and at temperature T ranging between -180 °C and 22 °C, as shown in Table 4.

The smooth tensile strength $\sigma_{B, RT}^{smooth}$ and notch strength σ_{B}^{notch} are expressed in Eq. (1). Here P_{max} = maximum load (kN) and d = test specimen diameter (4 mm).

$$\left.\begin{array}{l} \sigma_{B}^{smooth} = 4P_{max}/\pi d^{2} \\ \sigma_{B}^{notch} = 4P_{max}/\pi d^{2} \end{array}\right\} \tag{1}$$

In this study, the strain rate–temperature parameter R, given by Eq. (2), is used to evaluate the combined effects of strain rate and
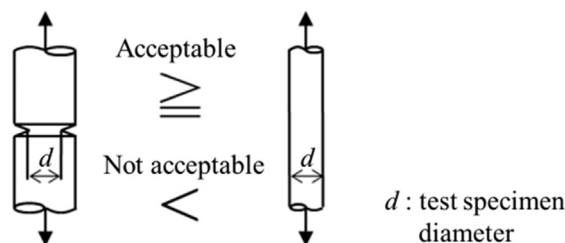

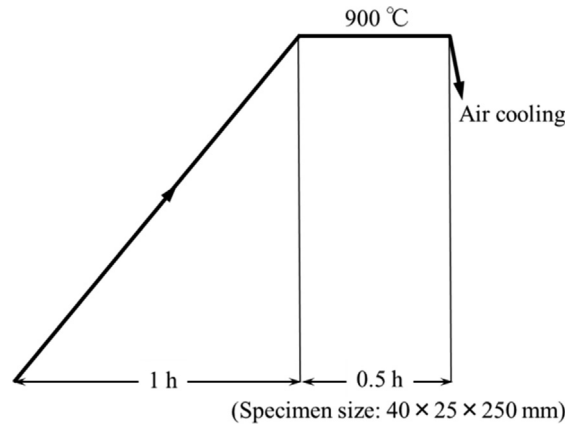Fig. 3. Comparison between smooth strength and notch strength.
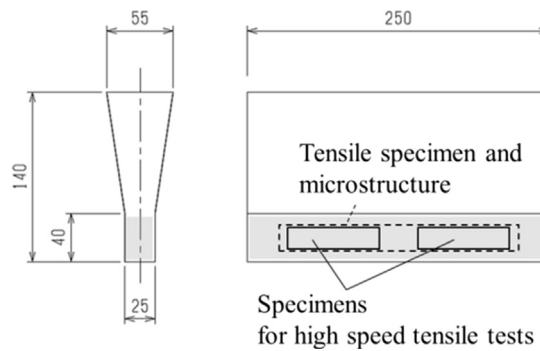
Fig. 4. Normalizing condition for PDI.

Fig. 5. Schematic view of JIS Type II Y–shaped block (in mm) and specimen positions.

Table 1
Chemical compositions of specimens (mass%).

Material	C	Si	Mn	P	S	Cu	Mg
High–Si ductile cast iron (As cast)	3.27	3.94	0.35	0.026	0.010	0.02	0.043
JIS-FCD500 (As cast)	3.75	2.08	0.40	0.021	0.004	0.24	0.044
JIS-FCD700 (As cast)	3.69	2.10	0.41	0.023	0.003	0.40	0.038
PDI (Normalizing)	3.66	2.09	0.41	0.024	0.004	0.73	0.041

Table 2
Microstructural characteristics of specimens.

Material	Average nodule diameter (μm)	Nodularity (%)	Graphite area fraction (%)	Pearlite area fraction of matrix (%)	Ferrite area fraction of matrix (%)
High–Si ductile cast iron (As cast)	26.9	90.2	10.4	0	100
JIS-FCD500 (As cast)	27.0	93.3	10.5	52.2	47.8
JIS-FCD700 (As cast)	26.0	95.8	10.1	83.6	16.4
PDI (Normalizing)	25.3	93.4	9.9	100	0

temperature on σ_B^{smooth} and σ_B^{notch}. The R parameter has been used until now to explain the influence of strain rate and temperature on the tensile strength and yield stress of steel [17–20]. Decreasing R parameter means increasing strain rate or decreasing temperature, or both. Then, deformation by dislocation motion becomes difficult with decreasing the R parameter.

$$R = T \times \ln(A/\dot{\varepsilon}) \tag{2}$$

Here T = temperature (K), $A = 10^8$ (s^{-1}) [17], $\dot{\varepsilon}$ is strain rate (s^{-1}), $\dot{\varepsilon} = \dot{\varepsilon}^{smooth}$ for smooth specimens, and $\dot{\varepsilon} = \dot{\varepsilon}^{notch}$ for notched specimens. The strain rate $\dot{\varepsilon}^{smooth}$ and $\dot{\varepsilon}^{notch}$ were calculated from the tensile speed $u(t)/t$, as given in Eq. (3).
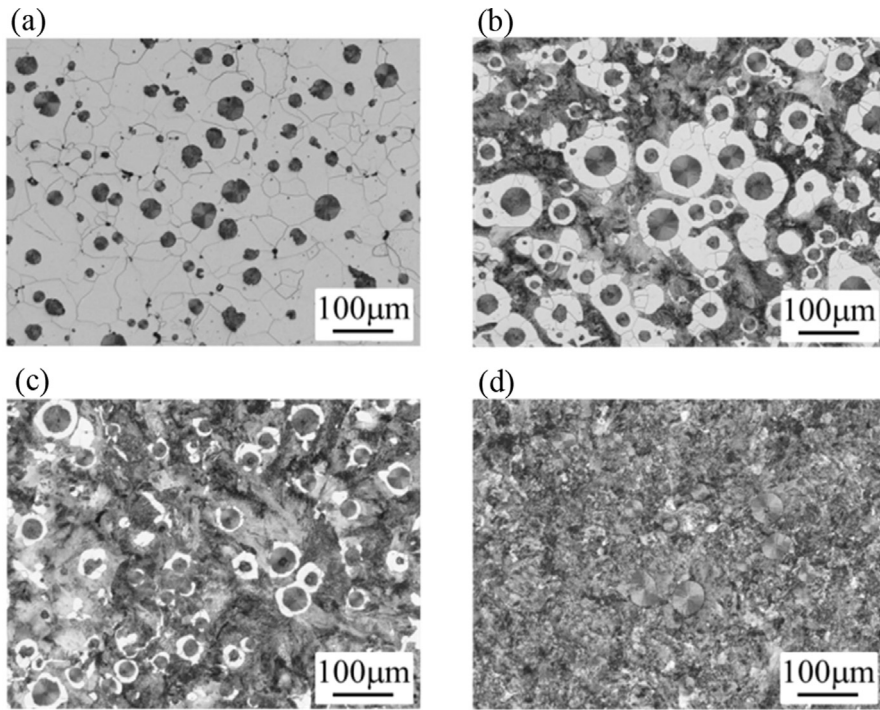
Fig. 6. Microstructures of specimens: high–Si ductile cast iron (a), JISFCD500 (b), JIS–FCD700 (c), and PDI (d).

Table 3
Tensile properties and Brinell hardness of specimens.

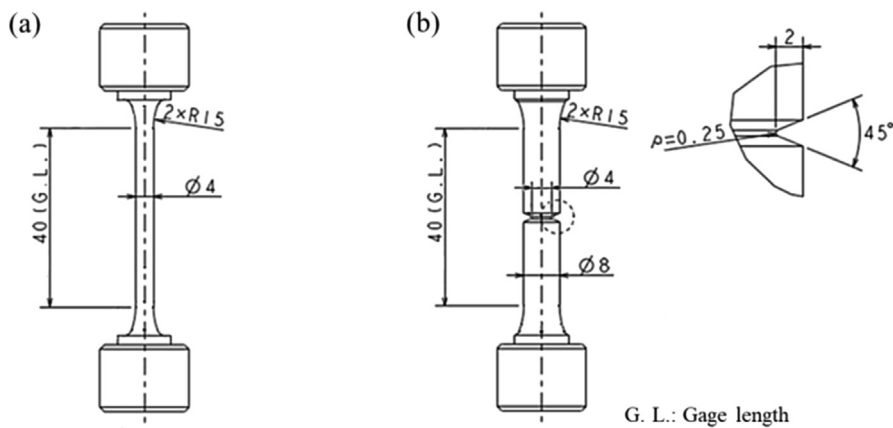| Material	Tensile strength σ_B (MPa)	Proof stress $\sigma_{0.2}$ (MPa)	Fracture strain ε_B (%)	Brinell hardness
High–Si ductile cast iron (As cast)	543	426	20	186
JIS-FCD500 (As cast)	566	323	11	190
JIS-FCD700 (As cast)	711	394	9	229
PDI (Normalizing)	933	573	7	293

Fig. 7. Configuration of high–speed tensile test specimen (in mm): smooth specimen (a) and notched round bar specimen (b).

$$\left. \begin{aligned} \dot{\varepsilon}^{\text{smooth}} &= (u(t)/t)/\ell \\ \dot{\varepsilon}^{\text{notch}} &= K_{t\dot{\varepsilon}} \times (u(t)/t)/\ell \end{aligned} \right\} \tag{3}$$

Here, $u(t)$ = stroke displacement (mm), t = time (s), and ℓ = gage length (40 mm). In this study, the stroke displacement applied at the specimen grip end was proportional to time t. The strain rate concentration factor $K_{t\dot{\varepsilon}}$ studied in our previous work [15,16] was used to calculate $\dot{\varepsilon}^{\text{notch}}$ owing to the difficulty in measuring the strain rate at notch root experimentally. Since the relation between the

Table 4
Temperature and strain rate condition used for the high–speed tensile test.

Material	Test No.	Notched specimen		Smooth specimen	
		Temperature T (°C)	Strain rate $\dot{\varepsilon}^{\mathrm{notch}}$ (s^{-1})	Temperature T (°C)	Strain rate $\dot{\varepsilon}^{\mathrm{smooth}}$ (s^{-1})
High–Si ductile cast iron	No. 1	25.0	2.03×10^{-3}	25.1	2.10×10^{-4}
	No. 2	24.7	1.97×10^{-1}	25.2	6.91×10^{-2}
	No. 3	24.7	4.35×10^{0}	25.2	5.01×10^{-1}
	No. 4	25.0	1.11×10^{1}	25.7	2.45×10^{0}
	No. 5	-42.9	1.97×10^{-3}	25.2	6.84×10^{0}
	No. 6	-42.6	2.00×10^{0}	-101.7	5.01×10^{-1}
	No. 7	-42.1	3.86×10^{0}	-130.5	5.00×10^{-1}
	No. 8	-99.6	3.78×10^{-3}		
	No. 9	-100.1	2.02×10^{-3}		
	No. 10	-100.5	1.96×10^{-2}		
	No. 11	-130.4	1.95×10^{-3}		
	No. 12	-129.4	3.90×10^{-3}		
JIS-FCD500	No. 1	25.1	2.02×10^{-3}	25.0	2.10×10^{-4}
	No. 2	25.7	2.02×10^{-3}	24.7	5.01×10^{-1}
	No. 3	25.6	4.25×10^{0}	25.2	6.49×10^{0}
	No. 4	25.7	1.75×10^{1}	-99.8	5.01×10^{-1}
	No. 5	-101.2	4.26×10^{0}	-181.7	6.86×10^{0}
	No. 6	-129.5	4.25×10^{0}		
	No. 7	-130.0	1.30×10^{1}		
JIS-FCD700	No. 1	25.0	1.99×10^{-3}	25.9	2.10×10^{-4}
	No. 2	24.8	4.33×10^{-3}	25.9	4.61×10^{-2}
	No. 3	24.7	4.13×10^{0}	25.9	4.82×10^{0}
	No. 4	24.9	1.75×10^{1}	-42.6	5.01×10^{-1}
	No. 5	24.4	1.78×10^{1}	-129.5	4.99×10^{-1}
	No. 6	-41.8	1.98×10^{-1}		
	No. 7	-40.8	4.34×10^{-1}		
	No. 8	-41.9	4.15×10^{0}		
	No. 9	-41.6	1.62×10^{1}		
	No. 10	-101.6	1.99×10^{-3}		
PDI	No. 1	25.8	2.00×10^{-3}	24.3	2.10×10^{-4}
	No. 2	25.8	3.07×10^{-1}	24.3	4.61×10^{-2}
	No. 3	25.8	4.35×10^{-1}	25.0	2.14×10^{0}
	No. 4	25.0	2.89×10^{0}	-11.1	5.00×10^{-1}
	No. 5	25.8	4.14×10^{0}	-40.2	5.00×10^{-1}
	No. 6	26.0	1.84×10^{1}	-128.8	5.00×10^{-1}

stress concentration factor and strain rate concentration factor was clarified in our previous study [15,16], the value of $K_t \dot{\varepsilon} = 9.49$ is very accurate for the notched specimen shown in Fig. 7(b) [15,16].

As shown in Fig. 7, the notch strength will be discussed by using the specific notch geometry similar to Charpy. This is because Charpy impact test has been used in many years as a unique method to ensure the safety of structures. By using the similar notch shape, an alternative method can be proposed by extending Charpy testing in more rational way. For example, impact bend loading in
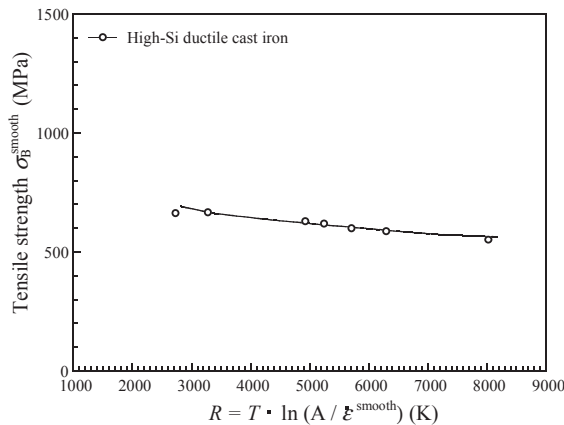

Fig. 8. Tensile strength $\sigma_B^{\mathrm{smooth}}$ of high–Si ductile cast iron in terms of parameter R.

Charpy is not suitable for machine design because the bending strength cannot be used conveniently in contrast to the tensile strength and the yield strength. Therefore, in this paper, a notched round bar specimen will be considered under high speed tensile test. Although several previous papers shows that the impact strength is affected by the notch shape [21–23], the obtained results may be useful for ensuring the safety of structures in a similar way of conventional Charpy testing.

3. Notch strength of high–si ductile cast iron in terms of R parameter

3.1. Tensile strength in terms of R parameter

In this study, the tensile strength and notch strength are considered in terms of the R parameter defined in Eq. (2). This parameter was proposed to explain the effects of strain rate and temperature on the tensile strength and yield stress of steel [17–20,24]. Bennett and Sinclair showed that the effects of strain rate and temperature on yield stress can be expressed in terms of the R parameter for steel and BCC metals [17], and Fujii et al. provided experimental proof for this statement [18–20,24].

Fig. 8 shows the tensile strength σ_B^{smooth} in terms of the R parameter for high–Si ductile cast iron. A good correlation can be seen between σ_B^{smooth} and R parameter at the strain rate ranging between 2.1×10^{-4} and $6.8 \times 10^{0} s^{-1}$ and temperature ranging between $-130 °C$ and $22 °C$. Here, a decreasing value of R means an increase in the strain rate or a decrease in temperature, or both. It can be seen that the tensile strength σ_B^{smooth} increases consistently with decreasing R in this experimental range.

3.2. Notch strength in terms of R parameter

Fig. 9 shows the notch strength σ_B^{notch} expressed in terms of R parameter for high–Si ductile cast iron. A unique σ_B^{notch} curve is obtained in the strain rate ranging between 2.0×10^{-3} and $1.1 \times 10^{1} s^{-1}$ and at temperature ranging between -130 and $22 °C$. With decreasing R value, σ_B^{notch} increases slightly in a similar way of σ_B^{smooth}, but σ_B^{notch} starts decreasing below $R = 4300 K$. As shown in Appendix C, the ductile dimple fracture surface disappears under $R < R_{th} \fallingdotseq 4300 K$. If ductile fracture surface disappears, σ_B^{notch} always decreases with decreasing parameter R. Fig. 9 also shows the static tensile strength at room temperature $\sigma_{B, RT}^{smooth}$. Except for the region of small R value, the notch strength σ_B^{notch} is higher than the tensile strength $\sigma_{B, RT}^{smooth}$ because of the notch–strengthening effect [25,26,27]. The stress–strain curves for smooth and notched specimens at the room temperature are given in Appendix A. All the materials considered in this study exhibit the notch–strengthening effect, as shown in Fig. 14. In Appendix B, σ_B^{notch} curves are indicated in terms of the strain rate. It can be seen that the σ_B^{notch} curves depend largely on the temperature. Compared to Fig. 15, Fig. 9 is very convenient to use because σ_B^{notch} is expressed as a master curve in terms of the parameter R.

3.3. Notch–strengthening threshold criterion $R \geqq R_{th}$ for $\sigma_B^{notch} \geq \sigma_{B, RT}^{smooth}$

The intersection of the σ_B^{notch} curve and $\sigma_{B, RT}^{smooth}$ line can be regarded as the notch–strengthening threshold R_{th}. The condition $\sigma_B^{notch} \geq \sigma_{B, RT}^{smooth}$ can be $R \geq R_{th}$. Under $R \geq R_{th}$, σ_B^{notch} is always higher than $\sigma_{B, RT}^{smooth}$. Therefore, if real products are used under the condition $R \geq R_{th}$, $\sigma_{B, RT}^{smooth}$ can be used as the strength of notched components in machine design safely and conveniently to prevent instantaneous fracture. The criterion $R \geq R_{th}$ provides the lowest service temperature and highest strain rate that can be applied to
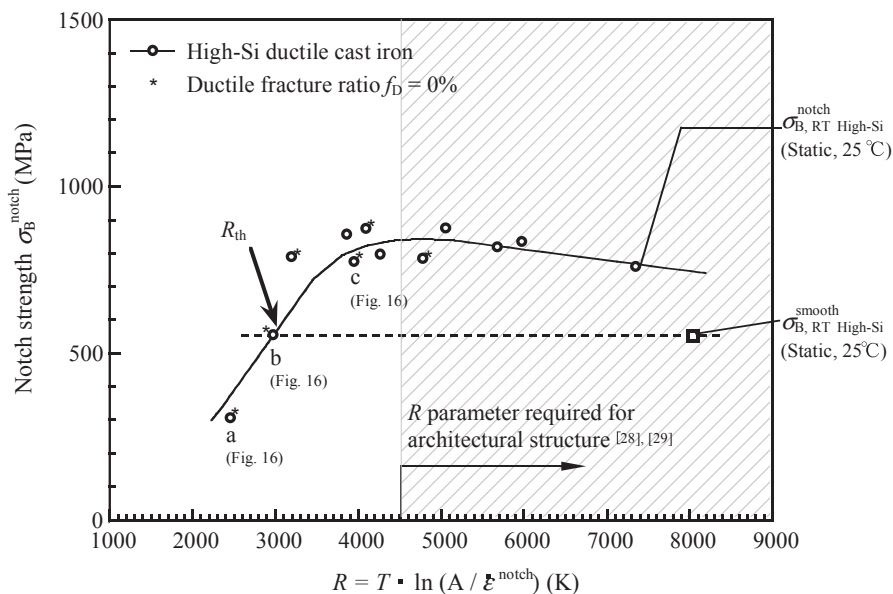

Fig. 9. Notch strength σ_B^{notch} of high–Si ductile cast iron in terms of parameter R.

structural components.

One may think that the threshold is not well defined since in Fig. 9 only one test result at an R value is less than threshold. However, as shown in Appendix C, under ductile fracture ratio $f_D = 0\%$ and notch strength σ_B^{notch} decreases with decreasing R. The fracture observation shows that σ_B^{notch} is always less than $\sigma_{B,RT}^{smooth}$ under $R < R_{th}$.

4. Notch strength of ferrite–pearlite ductile cast iron and safety verification through R_{th}

4.1. Tensile strength in terms of R parameter

Fig. 10 shows the tensile strength σ_B^{smooth} of JIS–FCD500, JIS–FCD700, and fully PDI. Each material has a unique σ_B^{smooth} curve in terms of the R parameter in the strain rate ranging between 2.1×10^{-4} and $6.9 \times 10^0 \, s^{-1}$ and temperatures ranging between $-180\,°C$ and $22\,°C$. It can be seen that the tensile strength σ_B^{smooth} increases consistently with decreasing R value in this experimental range. This tendency is consistent with that of high–Si ductile cast iron, as shown in Fig. 8.

4.2. Notch strength in terms of R parameter

Fig. 11 shows the notch strength σ_B^{notch} in terms of the parameter R for JIS–FCD500, 700, and PDI. The R curves are similar to those of high–Si ductile cast iron in Fig. 9. With decreasing R value, σ_B^{notch} increases but starts decreasing below $R = 2500$, 4200, and 5100 for JIS–FCD500, JIS–FCD700, and PDI, respectively. In Fig. 11, the static tensile strength at room temperature $\sigma_{B,RT}^{smooth}$ is indicated by broken lines. Therefore, the intersection of the σ_B^{notch} curve and $\sigma_{B,RT}^{smooth}$ line can be regarded as the notch–strengthening threshold R_{th}.

Conventional ductile cast iron JIS–FCD500 has been used widely in industrial applications. Although its Charpy absorbed energy is smaller, JIS–FCD700 has been used for several industrial applications, such as automotive underbody components, hydraulic components, and civil engineering and construction components. In this study, we have proposed the notch–strengthening threshold R_{th}. Under $R \geqq R_{th}$, σ_B^{notch} is always larger than $\sigma_{B,RT}^{smooth}$. Therefore, if real products are used under the condition $R \geqq R_{th}$, $\sigma_{B,RT}^{smooth}$ can be used as the notch strength safely and conveniently in machine design to prevent instantaneous fracture. One may think that the threshold is not well defined in Fig. 11 since only FCD700 shows results below the threshold. However, as shown in Appendix C, under ductile fracture ratio $f_D = 0\%$, notch strength σ_B^{notch} decreases with decreasing R. The fracture observation shows that σ_B^{notch} is always less than $\sigma_{B,RT}^{smooth}$ under $R < R_{th}$ for JIS-FCD500, 700 and PDI.

In Fig. 11, the notch strength is discussed by using the specific notch geometry similar to Charpy shown in Fig. 7. This is because Charpy impact test has been used in many years as a unique method to ensure the safety of structures. By using the similar notch shape, an alternative method can be proposed by extending Charpy in more rational way although several previous papers indicated that the impact strength is affected by the shape of the notch [20–22]. In a similar way of Charpy results used in many years, the obtained results as shown in Fig. 11 can be applied to ensuring the safety of structures.

4.3. Safety verification through notch–strengthening threshold criterion $R \geqq R_{th}$

In this section, we confirm the condition that $R \geqq R_{th}$ is satisfied in real products made of JIS–FCD500 and JIS–FCD700. These materials are used widely in industrial fields in a safe and sound manner; therefore, structural safety can be verified by confirming $R \geqq R_{th}$. Next, the criterion $R \geqq R_{th}$ is applied to other materials to investigate their safety in a similar way.

Table 5 shows the requirements of architectural structures, which are expressed as $R > 4522$ [28,29]. This is an example of the most severe requirement of structural components. Fig. 11 shows the R curves of JIS–FCD500 and JIS–FCD700 with the highlighted range of $R > 4522$. $R \geqq R_{th}$ is satisfied by both JIS–FCD500 and JIS–FCD700 under $R > 4522$. This is a good reason why
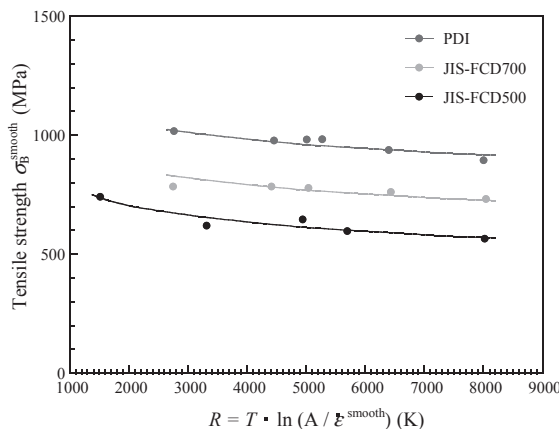

Fig. 10. Tensile strength σ_B^{smooth} of JIS–FCD500, JIS–FCD700, and PDI in terms of parameter R.
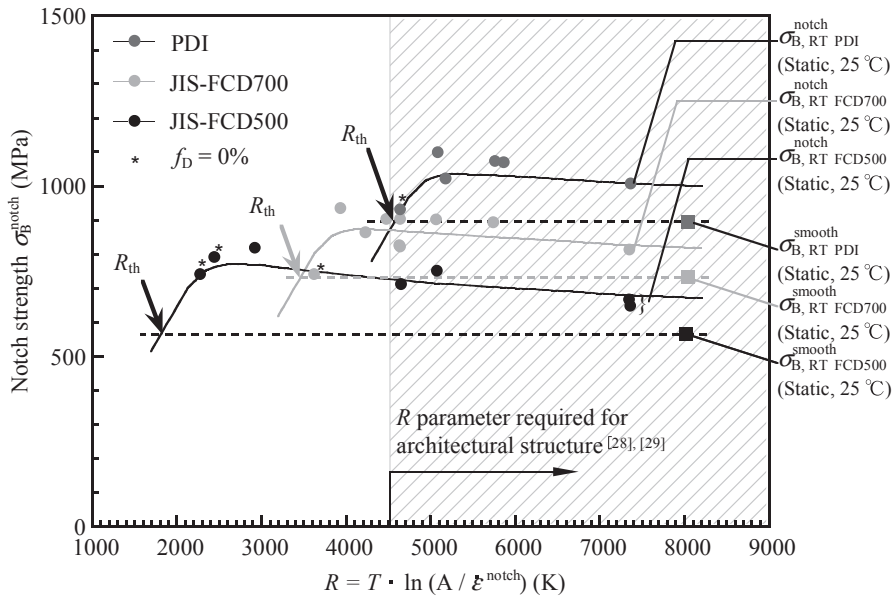
Fig. 11. Notch strength σ_B^{notch} of JIS–FCD500, JIS–FCD700, and PDI in terms of parameter R.

Table 5

Example of strain rate and temperature range acting on structural components.

Industrial field		Strain rate (s^{-1})	Temperature (°C)	R (K)
Design	Weld toes of beam-column (Architectural structure)	~2	−18~	4522~

JIS–FCD700 and JIS–FCD500 are used widely, although the value of Charpy absorbed energy is quite low. As stated earlier, if $R \geqq R_{th}$, $\sigma_{B,RT}^{smooth}$ can be used as the strength of notched components in machine design to prevent instantaneous fracture. Therefore, the notch–strengthening threshold criterion $R \geqq R_{th}$ can be conveniently used for judging the suitability of material, temperature and strain rate.

Finally, Figs. 9 and 11 show the R curves for high–Si ductile cast iron and PDI with $R > 4522$. As shown in Figs. 9 and 11, high–Si ductile cast iron totally satisfies the requirement and PDI almost satisfies $R \geqq R_{th}$. It may be concluded that the higher–strength ductile cast irons can be used for a wide range of strain rate and temperature, even though their Charpy absorbed energy values are smaller in comparison with those of the lower–strength ductile cast irons. Since the ductile cast iron considered in this paper exhibits a broad range of mechanical properties, the present approach and discussion can be applied for evaluating other high–strength materials under various temperature and strain rate.

5. Conclusions

In order to propose a useful evaluation method in structural design, which may replace Charpy impact testing, the notch strength σ_B^{notch} was discussed and compared with the static tensile strength at room temperature $\sigma_{B,RT}^{smooth}$. High–speed tensile tests were performed at stroke speed ranging between 8.5×10^{-3} and 2.7×10^2 mm/s (strain rates of 2.1×10^{-4}–1.8×10^1 s^{-1}) and at temperature ranging between -180 °C and 22 °C. The materials considered were high–Si ductile cast iron, conventional ferrite–pearlite ductile cast irons, and fully PDI. The strain rate–temperature parameter R was used for evaluating the combined influence of strain rate and temperature on strength. Our conclusions are as follows:

(1) Notch strength σ_B^{notch} can be expressed in terms of the R parameter as a unique master curve for each material independent of the temperature and strain rate (see Figs. 9 and 11). Then, the notch–strengthening threshold R_{th} was proposed to describe the lowest service temperature and highest strain rate that can be applied to structural components.

(2) If $R \geqq R_{th}$, notch strength σ_B^{notch} is always higher than the tensile strength $\sigma_{B,RT}^{smooth}$. Therefore, if the real products are under $R \geqq R_{th}$, their notch strength can be evaluated safely and conveniently using $\sigma_{B,RT}^{smooth}$ in mechanical design to prevent instantaneous fracture.

(3) Since the R_{th} values of high–Si ductile cast iron, JIS–FCD500, JIS–FCD700, and PDI satisfy the requirements of architectural structure [28,29], all components made of these materials can be used safely. It may be concluded that the high strength–grade ductile cast irons can be used over wide ranges of strain rate and temperature.

(4) Since the ductile cast iron considered in this paper exhibits a broad range of mechanical properties, the present approach and

discussion can be applied for evaluating other high–strength materials under various temperature and strain rate.

Appendix A. Stress–strain curves of notched and smooth specimens

Fig. 12 shows the stress–strain curves of smooth and notched round bar specimens obtained by a static tensile test at temperature $T = 25\,°C$ for high–Si ductile cast iron, JIS–FCD500, JIS–FCD700, and PDI. The maximum strength of the notched round bar specimen is higher than that of the smooth specimen, as shown in Fig. 12, for all materials. In previous studies, the notch–strengthening effects of ductile cast iron and steel were discussed [25,26]. It was explained that notch–strengthening may be affected by the multiaxial stress state at the notch root [25,26,27]. The multiaxial stress state is generated by the constraint of the deformation at the notch root area. This multiaxial stress state can be expressed as the triaxiality factor. The notch–strength of ductile cast iron and steel increase with increasing the triaxiality factor [25,26].

Appendix B. Notch strength σ_B^{notch} in terms of strain rate $\dot{\varepsilon}^{notch}$ depending on test temperature

Fig. 13 shows the relation between σ_B^{notch} and strain rate $\dot{\varepsilon}^{notch}$ at a temperature ranging between $-130\,°C$ and $25\,°C$ obtained from high–speed tensile test of high–Si ductile cast iron. In Fig. 15, σ_B^{notch} curves depend largely on the testing temperature. Using R parameter, however, the σ_B^{notch} curves in Fig. 13 can be expressed as a unique master curve, as shown in Fig. 9. Compared to Fig. 13,
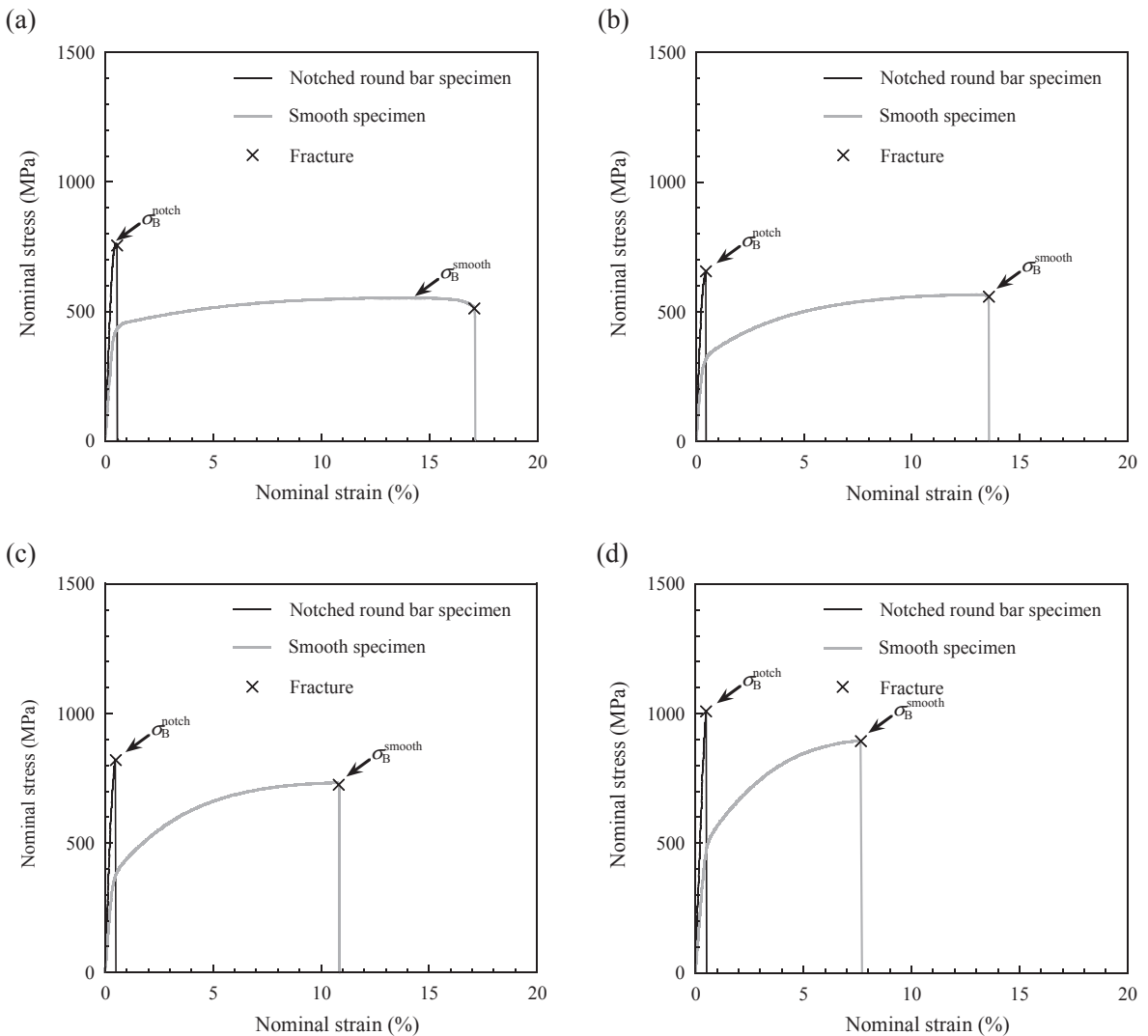

Fig. 12. Stress–strain curves of notched and smooth round bar specimens under static tensile test at temperature $T = 25\,°C$: high–Si ductile cast iron (a), JIS–FCD500 (b), JIS–FCD700 (c), and PDI (d).
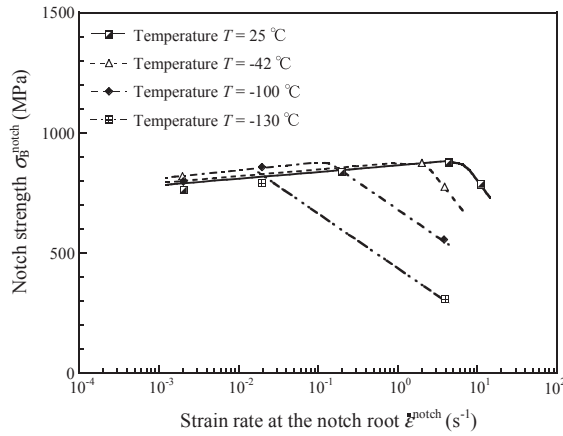
Fig. 13. Notch strength σ_B^{notch} of high–Si ductile cast iron in terms of strain rate $\dot{\varepsilon}^{notch}$ in temperature range of -130–25 °C.
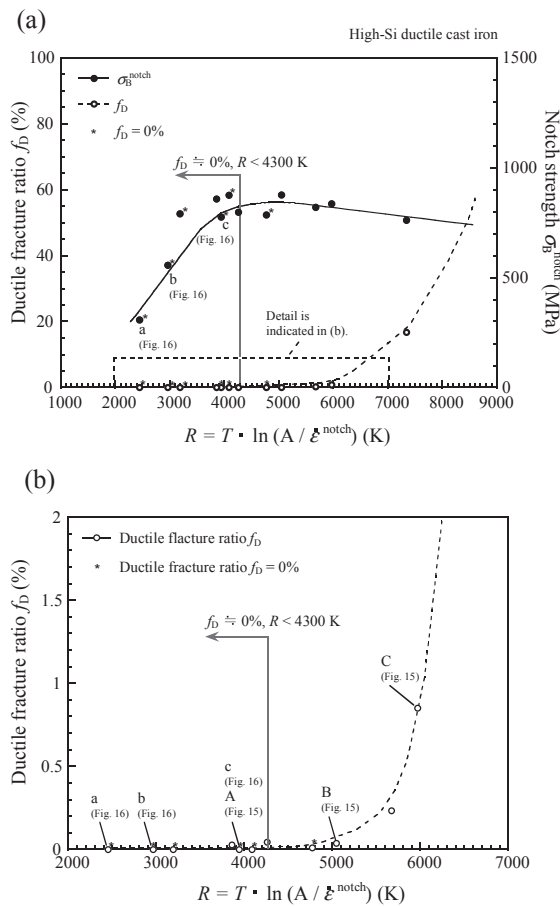

Fig. 14. Ductile fracture ratio on the notched specimen in comparison with σ_B^{notch} for high Si ductile cast iron: all data (a), enlarged view in the dotted line (b).

Fig. 9 is very convenient for use because σ_B^{notch} is expressed as a master curve independent of temperature and strain rate. The master curve expresses the ductile–brittle transition behavior uniquely in this test experimental range.

Appendix C. Ductile fracture ratio in terms of *R* parameter on the notched specimen

In Fig. 9, σ_B^{notch} starts decreasing below $R = 4300$ K. Fig. 14 shows the ductile fracture ratio f_D for high–Si ductile cast iron in
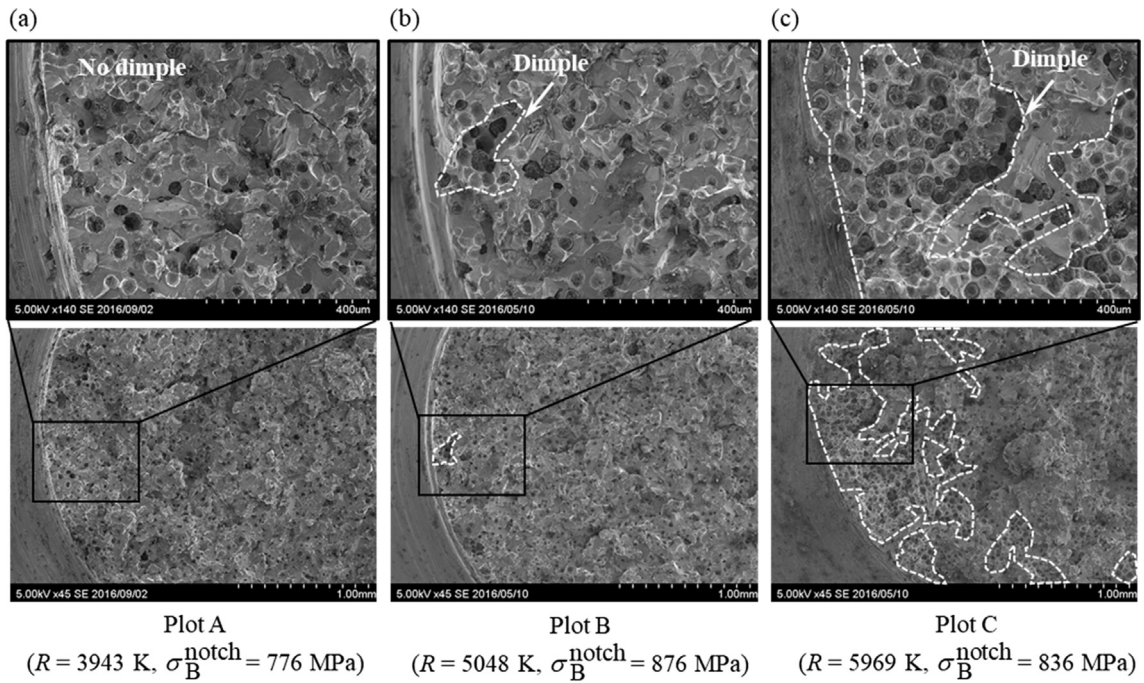
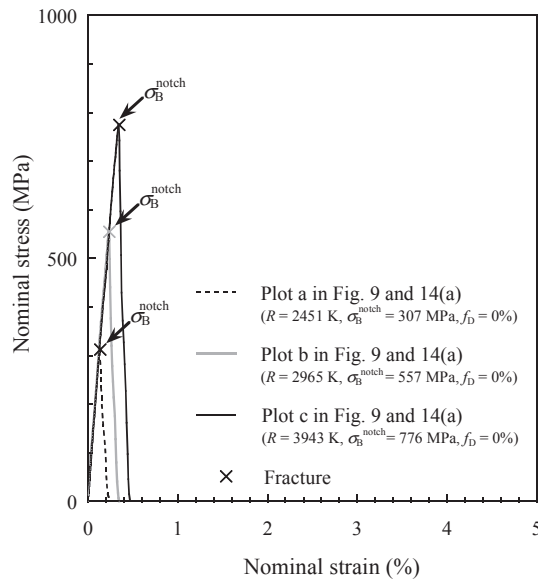Fig. 15. Fracture surfaces of plot A (a), plot B (b) and plot C (c) in Fig. 14(b).

Fig. 16. Stress–strain curves of plot a (a), plot b (b) and plot c (c) in Figs. 9 and 14.

comparison with σ_B^{notch}. Fig. 15 shows several fracture surfaces corresponding to the plot A, B and C in Fig. 14(b). As shown in Fig. 14, f_D decreases with decreasing parameter R. Finally, ductile dimple fracture disappears below $R \fallingdotseq 4300$ K. In Figs. 9 and 14, asterisk * denotes $f_D = 0\%$. By choosing several examples a, b, c in Figs. 9 and 14, Fig. 16 shows almost linear stress–strain curves for $f_D = 0\%$, which is quite different from Fig. 12. In the region of $f_D = 0\%$, σ_B^{notch} decreases with decreasing R. As shown in Fig. 14, under ductile fracture ratio $f_D = 0\%$, σ_B^{notch} decreases with decreasing R. The fracture observation shows that σ_B^{notch} is always less than $\sigma_{B, RT}^{smooth}$ under $R < R_{th}$ for high-Si ductile cast iron.

Fig. 17 shows the ductile fracture ratio f_D for JIS-FCD500, 700 and PDI in comparison with σ_B^{notch}. Similarly, in Fig. 17, under ductile fracture ratio $f_D = 0\%$, σ_B^{notch} decreases with decreasing R. In Fig. 17, small R value data may be insufficient. However, the fracture observation shows that σ_B^{notch} is always less than $\sigma_{B, RT}^{smooth}$ under $R < R_{th}$ for JIS-FCD500, 700 and PDI.
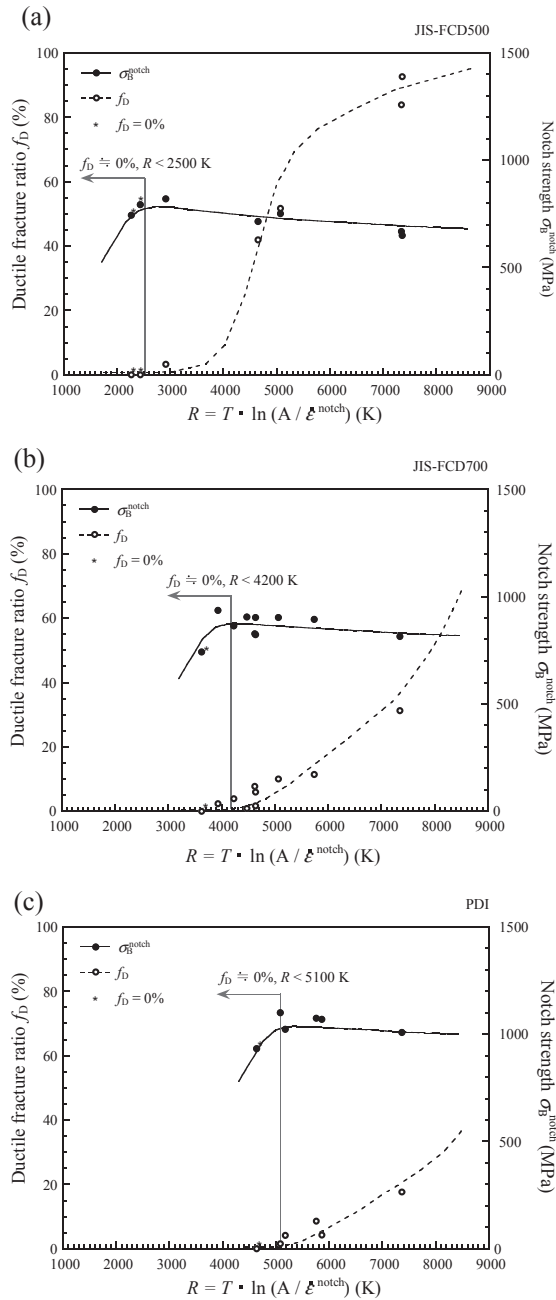
Fig. 17. Ductile fracture ratio on the notched specimen in comparison with $\sigma_{\mathrm{B}}^{\mathrm{notch}}$ for JIS–FCD500 (a), JIS–FCD700 (b), and PDI (c).

Appendix D. Supplementary material

Supplementary data to this article can be found online at https://doi.org/10.1016/j.engfracmech.2018.11.034.

References

[1] JIS–G5502. Spheroidal graphite iron castings. Tokyo, Japan; 2001.
[2] BS EN 1563. Founding–Spheroidal graphite cast irons. Brussels, Belgium; 2011.
[3] Larker R. Solution Strengthend Ferritic Ductile Iron ISO 1083/JS/500-10 Provides Superior Consistent Properties in Hydraulic Rotators. China Foundry 2009;6:343–51. Article ID: 1672-6421(2009)04-343-09.
[4] Larker R. Paradigm shift in revised EN 1563 (GJS) enables improved properties and production economy in both as-cast and austempered (ADI) states. Proc

NEWCAST Forum Dusseldorf, Germany 2011:29–34.

[5] Loblich H, Stets W, Einführung Die. non mischkristallverfestigem Gusseisen mit Kugeigraphit in die Industrie-eine Erfolgsstory. Proc Deutscher Gießjereitag; 2013 und 5 NEWCAST Forum, Fellbach, Germany 2013:14–7.

[6] Umetani T, Ikeda T, Sura N, Ashizuka K, Nemoto T, Takada H, et al. Tensile strength, fatigue strength, and impact strength of solution strengthened high silicon ferritic ductile cast iron. J JFS 2014;86:36–42.

[7] Ikeda T, Umetani T, Kai N, Noda N-A, Sano Y. Strain rate and temperature insensitiveness of notch-bend strength for high Si ductile cast iron. ISIJ Int 2016;56:868–74.

[8] Ikeda T, Umetani T, Kai N, Ogi K, Noda N-A, Sano Y. Influence of silicon content, strain rate and temperature on toughness and strength of solid solution strengthened ferritic ductile cast iron. Mater Trans 2016;57:2132–8.

[9] Yamamoto H, Kobayashi T, Fujita H. Strain rate dependency of ductile-brittle transition behavior in ductile cast iron. J JFS 2000;72:107–12.

[10] TverGaard V, Needleman A. An analysis of the temperature and rate dependence of Charpy V-notch energies for a high nitrogen steel. Int J Fract 1988;37:197–215.

[11] Bayoumi MR, Bassim MN. Temperature dependence of fracture toughness Jic and ductility for BCC materials in the transition region. Int J Fract 1983;23:259–69.

[12] Noda N-A, Ohtsuka H, Ando M, Sano Y, Takase Y, Shinozaki T, et al. Analysis of dynamic stress concentration and strain rate concentration for notched specimens used for high speed tensile test. Trans Jpn Soc Mech Eng 2013;79:1182–90.

[13] Ando M, Noda N-A, Kuroshima Y, Ishikawa Y, Takeda H. Impact properties of polydimethylsiloxane copolymerized polycarbonate and application of the time-temperature superposition principle. Trans Jpn Soc Mech Eng 2014;80:SMM0149. https://doi.org/10.1299/transjsme.2014smm0149.

[14] Noda N-A, Ohtsuka H, Zheng H, Sano Y, Ando M, Shinozaki T, et al. Strain rate concentration and dynamic stress concentration for double-edge-notched specimens subjected to high-speed tensile loads. Fatigue Fract Eng Mater Struct 2015;38:125–38.

[15] Noda N-A, Shen Y, Takaki R, Akagi D, Ikeda T, Sano Y, et al. Relationship between strain rate concentration factor and stress concentration factor. Theor Appl Fract Mech 2017;90:218–27. https://doi.org/10.1016/j.tafmec.2017.05.017.

[16] Noda N-A, Akagi D, Shen Y, Takaki R, Ikeda T, Sano Y, et al. Strain rate concentration factor in comparison with stress concentration factor of a circumferential notch in a round bar specimen. Trans Jpn Soc Mech Eng 2017;83:17–00034. https://doi.org/10.1299/transjsme. 17-00034.

[17] Bennett PE, Sinclair GM. Parameter representation of low-temperature yield behavior of body-centered cubic transition metals. Trans ASME 1966;65:518–24.

[18] Fuji E, Ohkuma Y, Kawaguchi Y, Tsukamoto M. Effects of temperature and strain rate on dynamic fracture toughness of steel. J Soc Nav Arch Jpn 1985;158:619–29.

[19] Goto K, Hirasawa H, Toyosada M. A simple estimating method of constitutive equation for structural steel as a function of strain rate and temperature. J Soc Nav Arch Jpn 1944;176:501–7.

[20] Yamamoto H, Kobayashi T, Fujita H. Strain rate-temperature dependency of impact tensile properties and ductile fracture behavior in ductile cast iron. Tetsu–to–Hagane 1999;85:765–70.

[21] Aoki M, Kiuchi A, Ikeda K. Evaluation of brittle fracture strength of circumferentially notched round bar under axial load. Tetsu–to–Hagane 1982;68:998–1007.

[22] Ishikawa N, Kobayashi Y, Toyoda M. Effect of loading rate on deformation and fracture properties of notched steels. Tetsu–to–Hagane 1988;88:121–6.

[23] Iino M, Ogasawara M, Mimura H. On transition behavior of low stress fracture mild steel. J High Press Inst Jpn 1977;15:179–84.

[24] Minami F, Hashida T, Toyoda M, Morikawa J, Ohmura T, Arimochi K, et al. Dynamic fracture toughness evaluation of structural steels based on the local approach. J Soc Nav Arch Jpn 1998;184:453–64.

[25] Noguchi T. Rupture strength of cast iron bar with circumferential notch. J Soc Mater Sci 1980;29:387–93.

[26] Majima T, Anzai M, Nakazawa H. Notch tensile strength of ductile materials. Trans Jpn Soc Mech Eng 1986;52:1171–6.

[27] Lei X, Li C, Shi X, Xu X, Wei Y. Notch strengthening or weakening governed by transition of shear failure to normal mode fracture. Scientific Reports 2015;5. https://doi.org/10.1038/srep10537. Article number: 10537 (2015).

[28] Okashita K, Ohminami R, Michiba K, Yamamoto A, Tomimatsu M, Tanji Y, et al. Investigation of the brittle fracture at the corner of P75 rigid-frame pier in Kobe harbor highway during the Hyogoken-Nanbu earthquake. J Jpn Soc Civ Eng 1998;591:243–61.

[29] Toyoda M. Lessons learned from great Hanshin earthquake for steel framed structures with particular reference to materials/welding. Mater Jpn 1996;35:370–9.